Defence Technology xxx (xxxx) xxx

Contents lists available at ScienceDirect

Defence Technology

journal homepage: www.keaipublishing.com/en/journals/defence-technology

Numerical simulation of flow field characteristics and the improvement of pressure oscillation of rotating detonation engine

Xin-pei Han [a], Quan Zheng [a, *], Bao-xing Li [b], Qiang Xiao [a], Han Xu [a], Fang Wang [a], Hao-long Meng [a], Wen-kang Feng [a], Chun-sheng Weng [a]

[a] National Key Laboratory of Transient Physics, Nanjing University of Science and Technology, Nanjing, 210094, China
[b] Xi'an Modern Chemistry Research Institute, Xi'an, 710065, China

ARTICLE INFO

Article history:
Received 8 March 2022
Received in revised form
11 May 2022
Accepted 15 June 2022
Available online xxx

Keywords:
Detonation flow field
Combined chamber
Pressure oscillation
Velocity vector

ABSTRACT

Due to the inherent working mode of rotating detonation engine (RDE), the detonation flow field has the characteristics of pressure oscillation and axial kinetic energy loss, which makes it difficult to design nozzle and improve propulsion performance. Therefore, in order to improve the characteristics of detonation flow field, the three-dimensional numerical simulation of annular chamber and hollow chamber is carried out with premixed hydrogen/air as fuel in this paper, and then tries to combine the two chambers to weaken the oscillation characteristics of detonation flow field through the interaction of detonation flow field, which is a new method to regulate the detonation flow field. The results show that there are four states of velocity vectors at the outlet of annular chamber and hollow chamber, which makes RDE be affected by rolling moment and results in the loss of axial kinetic energy. In the external flow field of combined chamber, the phenomenon of cyclic reflection of expansion wave and compression wave on the free boundary is observed, which results in Mach disk structure. Moreover, the pressure monitoring points are set at the external flow field. The pressure signal shows that the high-frequency pressure oscillation at the external flow field of the combined chamber has been greatly weakened. Compared to the annular chamber, the relative standard deviation (RSD) has been reduced from 14.6% to 5.6%. The results thus demonstrate that this method is feasible to adjust the pressure oscillation characteristics of the detonation flow field, and is of great significance to promote the potential of RDE and nozzle design.

1. Introduction

Detonation wave is a supersonic combustion wave characterized by the leading shock closely coupled with the trailing reaction. It is extremely high heat release rate that makes detonation combustion close to constant volume combustion, and the thermos-cycle efficiency of propulsion device based on detonation combustion is higher [1]. As an application form of detonation propulsion, RDE (Rotating Detonation Engine) not only inherits the advantages of detonation combustion, but also holds the characteristics of compact structure and wide working range, thereby exhibiting broad application prospects [2–4]. As a propulsion device, the world-wide researchers make efforts to realize stable and efficient detonation combustion and maximize the heat energy released into mechanical energy. However, in the process of in-depth researches, it is found that there are some characteristics of detonation flow field that makes the energy released through detonation combustion hard to be converted into mechanical energy.

In the 1960s, Voitsekhovskii of Russia observed the flow field structure of rotating detonation waves in a disc-shaped chamber for the first time [5]. Nicholls et al. [6] of the United States used different gaseous fuels and oxygen as oxidant to obtain transient rotating detonation waves. Subsequently, through a large number of experimental and numerical simulation researches, it is found that the detonation flow field has the characteristics of high-frequency pressure oscillation, and there is non-axial velocity vector at the outlet, which brings some difficulties in the efficient utilization of energy [7–15]. Rankin et al. [16] found that when the

* Corresponding author.
E-mail address: q.zheng@njust.edu.cn (Q. Zheng).
Peer review under responsibility of China Ordnance Society

https://doi.org/10.1016/j.dt.2022.06.005

Nomenclature

$F_{chamber}$	thrust generated by the outlet of chamber
F_{wall}	thrust generated by the end face of the chamber
F_{total}	total thrust
p_{exit}	static pressure at the outlet of the chamber
ρ_{exit}	gas density at the outlet of the chamber
p_b	ambient pressure
p_{wall}	pressure on the end face of the chamber
I_{sp}	specific impulse
$\dot{m}$	mass flow rate
g	gravity acceleration 9.81 m/s^2
M_{gas}	moment of exhausted gas
$M_{chamber}$	moment of the chamber
r	force arm
$v_{tangential}$	tangential velocity at the outlet
v_{axial}	axial velocity at the outlet
v_{radial}	radial velocity at the outlet
E_{axial}	axial proportion of kinetic energy
$E_{tangential}$	tangential proportion of kinetic energy
E_{radial}	radial proportion of kinetic energy
RSD	relative standard deviation
p_i	ith pressure
$\overline{p}$	time-average pressure
N	total number of value point

mass flow is low, there is high-frequency pressure oscillation in the gas gathering chamber. Anand et al. [17] found that in addition to the main frequency of detonation wave propagation, there is an inherent low-frequency pressure oscillation in the combustion chamber. Ishihara et al. [18] pointed out that the high-frequency characteristics of flow field lead to many unsolved problems in the RDE, and the outlet state of the combustion chamber is very complex. Sun et al. [19,20] found that there is non-axial velocity vector at the outlet of the combustion chamber in the three-dimensional numerical simulations of RDE, which will result in a certain loss of axial kinetic energy. At the same time, they found that the higher ambient pressure is, the stronger oscillation characteristics of the external flow field are. And this oscillation will increase the instability of thrust, especially when the mass flow rate is low. Schwer et al. [21] simulated the flow field at the outlet of the annular chamber with the central cone and found that the oblique shock wave in the chamber formed complex shock after contacting the central cone and rebounded near the outlet flow field of the annular chamber.

The mentioned problems of flow field uneven, axial kinetic energy loss and thrust instability are caused by the characteristics of detonation flow field. Now, this situation is generally improved through the design of nozzle [22–25]. On the other hand, the high-frequency pressure oscillation of the flow field also presents difficulties in the design of RDE nozzles. Frolov et al. [26] studied the propulsion performance of RDE with nozzle and found that the specific impulse performance of RDE was 6–8% higher under the same injection conditions. Schnabel et al. [27] used the traditional steady-state method to design the RDE plug nozzle, and pointed out that there is no nozzle design rule to meet this unsteady and transient flow field. Wei et al. [28] studied an engine coupled with turbine guide vane and found that the pressure oscillation characteristics decreased to a certain extent when the oblique shock swept through turbine guide vane. Rankin et al. [8] also tried to solve the problem of high-frequency oscillation of detonation flow field by combining central cone and laval nozzle. The experimental results show that this problem has been solved to a certain extent. Huang et al. [29] proposed a plug nozzle design method by combining the characteristic line method and Mach line method, and simulated the unstable flow field at the outlet of the combustion chamber in detail, discussed the feasibility of unsteady nozzle design according to the air velocity angle and shock dynamic characteristics, and analyzed the influence of plug nozzle on air velocity angle and propulsion performance. It is concluded that the unsteady flow field characteristics exist whether the nozzle is installed or not, which will make the nozzle unable to achieve the best design state. However, nozzle is the key structure for the engine to convert heat energy into mechanical energy. The design of the nozzle directly affects the performance of RDE, it is thus significant to improve the unsteady flow field characteristics of RDE.

Since the effect of using a fixed mechanical structure to adjust the high-frequency oscillations of detonation flow field is always limited, the idea of using fluid to adjust the flow field came into being. This idea has been preliminarily verified on Plus Detonation Engine (PDE) by injecting air flow to adjust the under-expansion and over-expansion state of detonation flow field. Zhang et al. [30,31] successfully adjusted the expansion characteristics and obtained better propulsion performance through secondary flow injection in the throat and expansion section of a Laval nozzle. And they also verified the possibility of vector control through the injected air flow, which preliminarily proved that the method of fluidic regulation is feasible for the detonation flow field with high-frequency oscillation. Up to now, this novel method has not been adopted in RDE yet to adjust the flow field dynamics.

In addition, the thrust of the traditional annular RDE will decrease due to the end face of the inner cylinder [20]. In recent years, hollow RDE has gradually become a popular topic. Tang et al. [32] proposed the model of hollow chamber earlier, and realized the stable propagation of detonation wave in numerical simulation. Xia et al. [33] studied the wave system evolution process from ignition to stability in a hollow chamber through three-dimensional numerical simulation, and considered that the fresh premixed fuel layer plays an important role in the stability of detonation wave. Liu et al. [34] found the shock wave propagating backward with the detonation wave by establishing the injection structure of hollow chamber in detail, and analyzed the propagation mechanism between them in detail. Anand et al. [35] also made a detailed analysis of the flow field in hollow chamber and believed that one reason for the high-frequency instability was the superposition of multiple physical factors. In experiment, through the combustion chamber made of transparent glass, the internal flow field structure of hollow chamber has been observed [36–38]. Peng et al. [39] obtained stable detonation flow field by using hydrogen/air, ethylene/air and methane/air as fuel, and carried out quantitative analysis methods to find out that the hollow chamber has smaller velocity loss. Wang et al. [40] experimentally compared the hollow chamber with the annular chamber and found that the hollow chamber has better detonation performance and higher pressure gain. And some experimental and numerical simulation researches were carried out on hollow chamber with nozzle [38,41,42].

In order to change the unstable characteristics of pressure oscillation of RDE flow field, based on the idea of fluidic regulation

and combined with the advantages of hollow chamber, a combined chamber is simulated in this paper. The purpose is to change the pressure oscillation characteristics of detonation flow field through the interaction of outlet flow field of annular chamber and hollow chamber, and make use of the space in the middle of the annular chamber to make the engine more compact. In this paper, the annular RDE, hollow RDE and combined RDE are simulated in detail, the internal and external flow field structures of each example are analyzed, the flow field parameters are compared, and their performance is discussed.

2. Methodology

2.1. Physical model

In this paper, the Cartesian coordinate system is adopted, the central point of the hollow chamber inlet plane is selected as the coordinate origin, and the Z axis is the axial direction. Three cases are calculated, namely Case 1: annular chamber, Case 2: hollow chamber, Case 3: combined chamber. The physical models of the three cases are illustrated in Fig. 1, and the physical models of each example on the figure are schematic diagrams. In Fig. 1(a), the inner radius r_1 is 25 mm, the outer radius r_2 is 30 mm, the length l_1 is 50 mm, the wall thickness of the chamber is 5 mm, and the external flow field is a cylindrical area with a length of 300 mm and a diameter of 100 mm. In Fig. 1(b), the overall radius r_1 of Case 2 is 25 mm (the same as the inner radius of Case 1), in which the radius of the hollow chamber is 20 mm, the thickness of the wall is 5 mm. The premixed gas injection inlet is a ring with a width of $w_1 = 10$ mm, and the length l_1 of the chamber and the size of the external flow field are the same as case 1. In Case 3, the size of annular chamber, hollow chamber and external flow field are completely consistent with Case1 and Case 2, it is a combined chamber with wall thickness of 5 mm respectively, as showed in Fig. 1(c).

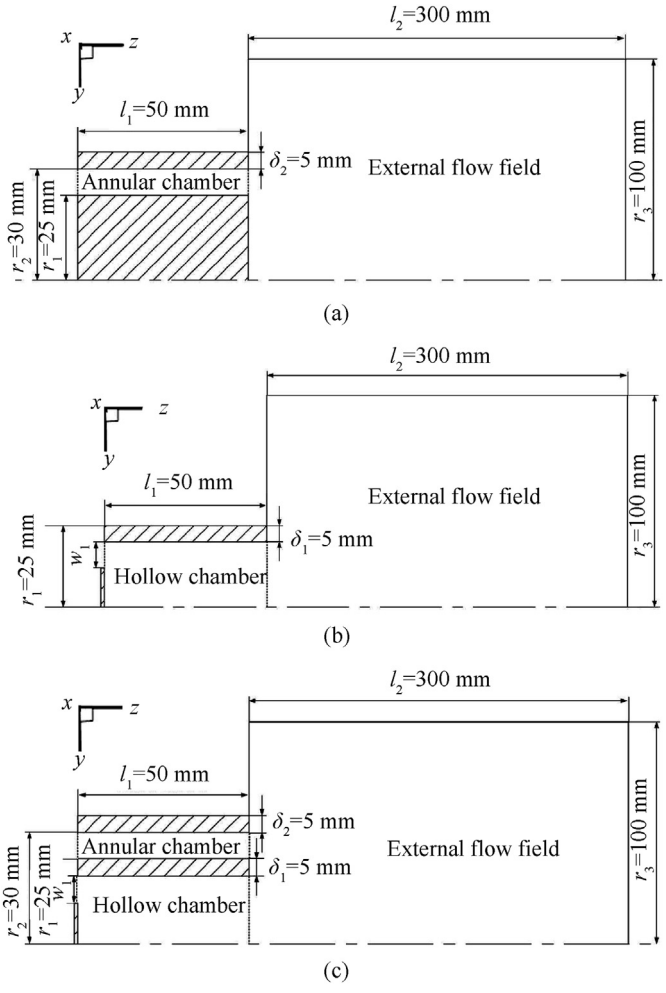

Fig. 1. Physical model: (a) Case 1: Annular chamber; (b) Case 2: Hollow chamber; (c) Case 3: Combined chamber.

2.2. Computational domain and boundary conditions

As showing in Fig. 2, each case is divided by structured grid. In detonation simulation, it usually required several points in a half reaction length to capture the detailed cellular structure of the detonation front, which is far beyond the current computing capability. In the present work, the purpose is to study the flow field structure. According to previous studies, the grid size of 0.2–0.5 mm is fine enough to capture the flow field structure [42–49]. Therefore, for the combustion chamber, a grid with an average size of 0.3 mm is used to simulate the mainstream field, and we further refine the grid near the wall. The grid size of the first layer is set to 0.02 mm, and gradually increases to the grid size of the mainstream field when the growth rate is 1.2, so as to meet the requirements of the turbulence model for the boundary layer [42]. For the external flow field, the change rate of flow parameters at the outlet of the chamber is relatively large, thus a finer grid size is needed to capture the change of flow parameters. As the change rate of flow parameters far from the chamber is relatively small. We then optimize the grid of the external flow field. Near the outlet, we adopted the same grid size of 0.3 mm as the mainstream field in the internal flow field. When it is far away from the outlet of the combustion chamber, the grid size gradually increases, and a coarser grid size is used. This grid treatment method has proved to be feasible in the previous study of detonation external flow field [50–52]. For the treatment of inlet boundary conditions, we adopted the method of fixing its mass flow rate. In Case 1, the mass flow rate at the inlet is 0.2 kg/s and the total temperature is 300 K. In Case 2, the mass flow rate at the inlet is 0.3 kg/s and the total temperature is 300 K. The inlet conditions in Case 3 are the same as those in Case 1 and Case 2. The total injection pressure at each inlet is matched according to the specific parameters of each case. This treatment method is closer to the experimental condition, because we are more concerned about the mass flow rate into RDE for pressurization operation in the experimental process [29,42]. For the wall, we used the adiabatic non slip boundary condition. The chamber outlet is directly connected with the external flow field area. We set the external flow field boundary as the pressure outlet boundary [53–55], with the pressure and temperature on the boundary assigned with reference to the atmospheric parameters, which are 0.1 MPa and 300 K respectively. When the boundary is in subsonic state, the outlet pressure is equal to the external ambient pressure. When the boundary is in supersonic state, the flow state at the outlet boundary is extrapolated from the internal flow field [56].

2.3. Numerical method and verification

In this paper, the detonation flow field in each case was solved based on the Reynolds averaged Navier-Stokes (RANS) method. In the Cartesian coordinate system, the tensor representation method of RANS is as follows:

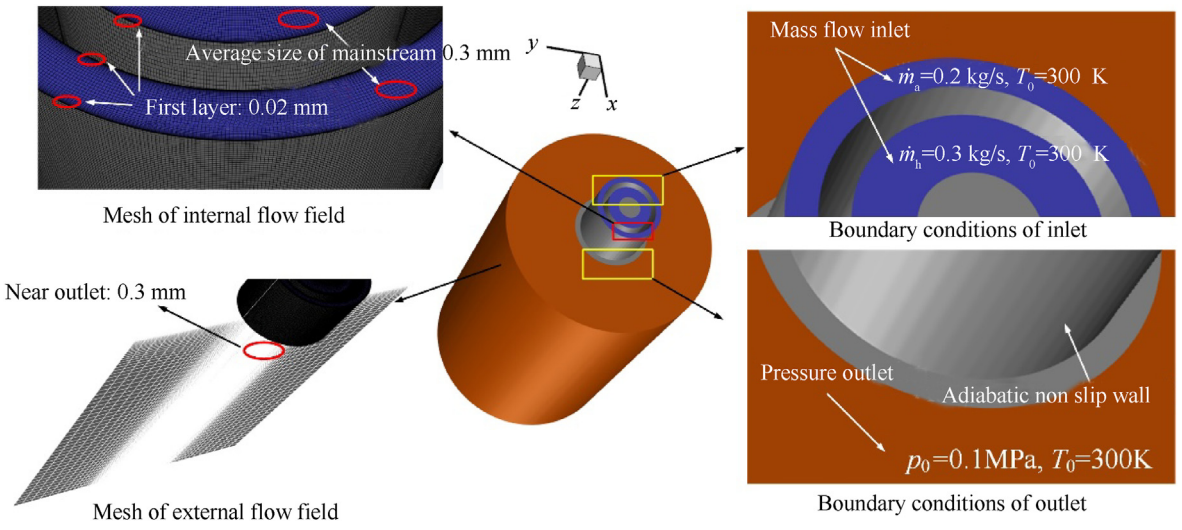

Fig. 2. Computing domain division and boundary conditions.

$$\frac{\partial \rho}{\partial t}+\frac{\partial}{\partial x_i}(\rho u_i)=0 \tag{1}$$

$$\frac{\partial}{\partial t}(\rho u_i)+\frac{\partial}{\partial x_j}(\rho u_i u_j)=-\frac{\partial p}{\partial x_i}+\frac{\partial}{\partial x_j}\left[\mu\left(\frac{\partial u_i}{\partial x_j}+\frac{\partial u_j}{\partial x_i}-\frac{2}{3}\delta_{ij}\frac{\partial u_l}{\partial x_l}\right)\right]+\frac{\partial}{\partial x_j}\left(-\rho\overline{u_i' u_j'}\right) \tag{2}$$

In the above equation, ρ is the density, t is the time, u_i is the Reynolds mean velocity without the mean sign, p is the pressure, δ_{ij} is the Kroneker tensor component, u_i' is the pulsating velocity.

For the turbulence modeling, the shear stress transfer(k-ω) model is used [67], which is sufficient to solve the flow field structures such as shock wave and expansion wave in detonation flow field [19]. k-ω two equation model mainly solves the turbulent flow energy k and its specific dissipation rate ω. The specific form of the convection transport equation is as following:

$$\frac{\partial(\rho k)}{\partial t}+\frac{\partial}{\partial x_j}\left[\rho u_j k-(\mu+\sigma_k\mu_t)\frac{\partial k}{\partial x_j}\right]=\tau_{tij}-\beta^*\rho\omega k \tag{3}$$

$$\frac{\partial(\rho\omega)}{\partial t}+\frac{\partial}{\partial x_j}\left[\rho u_j\omega-(\mu+\sigma_\omega\mu_t)\frac{\partial \omega}{\partial x_j}\right]=p_\omega-\beta\rho\omega^2+2(1-F_1)\frac{\rho_{\omega 2}}{\omega}\frac{\partial k\partial\omega}{\partial x_j\partial x_j} \tag{4}$$

where k is turbulent flow energy, ω is specific dissipation rate, μ_t is the eddy viscosity, F_1, β^*, σ_k, σ_ω, p_ω, β are model constant that adopted according to Menter's work [67]. And the eddy viscosity model of Reynolds stress is

$$\tau_{tij}=2\mu_t\left(S_{ij}-\frac{1}{3}S_{nn}\delta_{ij}\right)-\frac{2}{3}\rho k\delta_{ij} \tag{5}$$

where S_{ij} is the average velocity strain rate tensor.

The chemical reaction in this paper is H_2/air one-step reaction ($2H_2+O_2+3.76N_2=2H_2O+3.76N_2$). The reaction model contains four species including H_2, O_2, H_2O and N_2, which are widely used in the numerical simulation of detonation flow field [57–61]. The chemical reaction rate is calculated by Arrhenius formula, and various constants are applied according to the work of *Ma* et al. [61]. In order to capture the strong discontinuity such as detonation wave and oblique shock wave, the flux term is split by Roe-FDS scheme, the convection term is discretized by second-order upwind scheme, and time is advanced by second-order implicit scheme.

In order to verify the grid independence, three mesh sizes of mainstream (fine mesh: 0.2 mm, medium mesh: 0.3 mm, coarse mesh: 0.4 mm) of annular chamber are used to verify the numerical method. Among the three mesh sizes, the thickness of the first boundary layers are 0.02 mm, and the total number of grids is 8.73 million, 3.46 million and 1.52 million respectively. Fig. 3 shows pressure and temperature distribution along the circular curve (z = 2 mm, r = 27.5 mm) at the inlet of the combustion chamber with three grid sizes at t = 530 μs. It can be seen from the figure that the pressure and temperature distributions with different grid sizes are almost the same, indicating that there is almost no difference in the detonation wave with the three grid sizes. Considering that the specific detonation cellular structure is not studied in this paper, and the medium grid size is enough to capture the detailed structure of detonation flow field, the following simulations thus adopted the medium grid for calculation.

Fig. 4 shows the comparison between the experimentally observed detonation wave and the simulation results in this paper. It can be found that the simulation results are almost consistent with the detonation wave shape observed in the experiment. Comparison of the stable detonation parameters and the detonation parameters calculated by NASA CEA program is shown in Table 1. The initial pressure and temperature are 0.17 MPa and 286 K, respectively. The results show that the difference between the numerical value and the theoretical value of CJ is within 5%. Considering the loss such as lateral expansion of detonation wave, it can be considered that the simulation method of this study is feasible. In addition, accumulated errors will occur during the unsteady state calculation. It is generally accepted that the upper limit of allowable accumulation error is between 1 and 5%. In this study, the time step is set to 0.05 μs, and the total simulation time is 3 ms. According to the estimation of reference [63,64], the accumulated error generated in is 0.1%, which is far from reaching allowable accumulation error 1–5%, ensuring the reliability of unsteady calculation results.

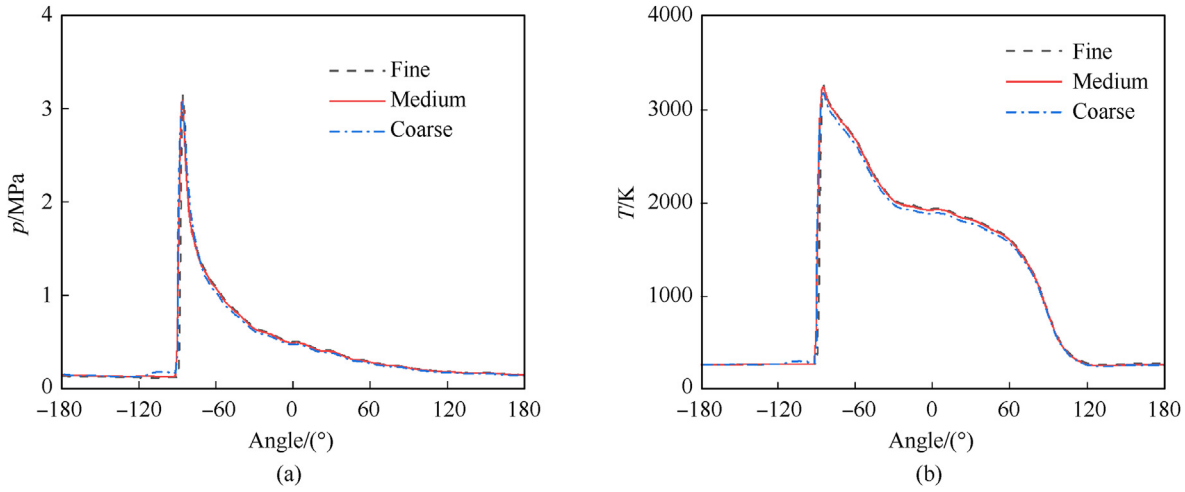

Fig. 3. Pressure and temperature distributions on curve ($z = 2$ mm, $r = 27.5$ mm) at $t = 530$ μs: (a) Pressure; (b) Temperature.

Fig. 4. Comparison of detonation wave structure between experimental and numerical results: (a) Experimental result [62]; (b) Simulation result.

Table 1
Comparison of detonation parameter between numerical values and C-J theoretical value.

	Detonation pressure/MPa	Detonation temperature/K	Detonation wave velocity/(m·s^{-1})
Theoretical value	2.88	3160	1967
Numerical value	2.79	3124	1889
Deviation	3.1%	1.4%	4.1%

3. Results and discussion

In this section, the calculation results of Case 1 - Case 3 will be demonstrated. For Case 1 and Case 2, we mainly analyze their internal flow field structure and their propulsion performance respectively. For Case 3, we mainly concentrate on the external flow field structure after interaction and the comparison of propulsion performance after combination. The ignition mode of three cases in this paper adopts the idealized mode, that is, the one-dimensional Chapman-Jouguet detonation parameter is set as the ignition and detonation condition at the head of the combustion chamber [33]. The mass flow rate of annular chamber is 0.2 kg/s, there is only one detonation wave in the combustion chamber. And the mass flow rate of hollow chamber is 0.3 kg/s, there are three detonation waves in the combustion chamber finally.

3.1. Annular chamber

The three-dimensional chamber is unwrapped into a two-dimensional plane along the outer wall, and the flow field in the annular chamber is obtained as shown in Fig. 5. Fig. 5(a) shows the pressure and temperature contours after the flow field becomes stable. In the temperature contours, it can be noted that the flow field structure of the annular chamber is a typical single wave structure, including detonation wave, oblique shock wave, slip line and triangular fresh mixture layer. The internal flow field structure is similar to our previous research work [65]. Fig. 5(b) shows the pressure curve detected at the monitoring point with coordinates (0, 29, 2) near the outer wall of the chamber inlet during the process from initiation to being stable. It can be seen that after the second peak, the pressure value of the detonation wave passing through the monitoring point is almost unchanged, indicating that the detonation wave has reached a stable state, and the pressure peak after stability is 2.7 MPa. By utilizing the last four cycles in the figure for wave velocity calculation, it can be found that the time between four peaks is 368.6 μs. The wave velocity in the annular chamber is 1875.1 m/s.

After the premixed gas is swept by the detonation wave in the combustion chamber, a large amount of heat energy will be released, and the high-temperature and high-pressure gas in the combustion chamber will be discharged from the outlet of the chamber and generate thrust. The thrust and specific impulse generated by RDE is calculated as following:

$$F_{\text{chamber}} = \iint_{\text{exit}} \left(\rho_{\text{exit}} v_{\text{axial}}^2 + p_{\text{exit}} - p_{\text{b}}\right) \mathrm{d}A \tag{6}$$

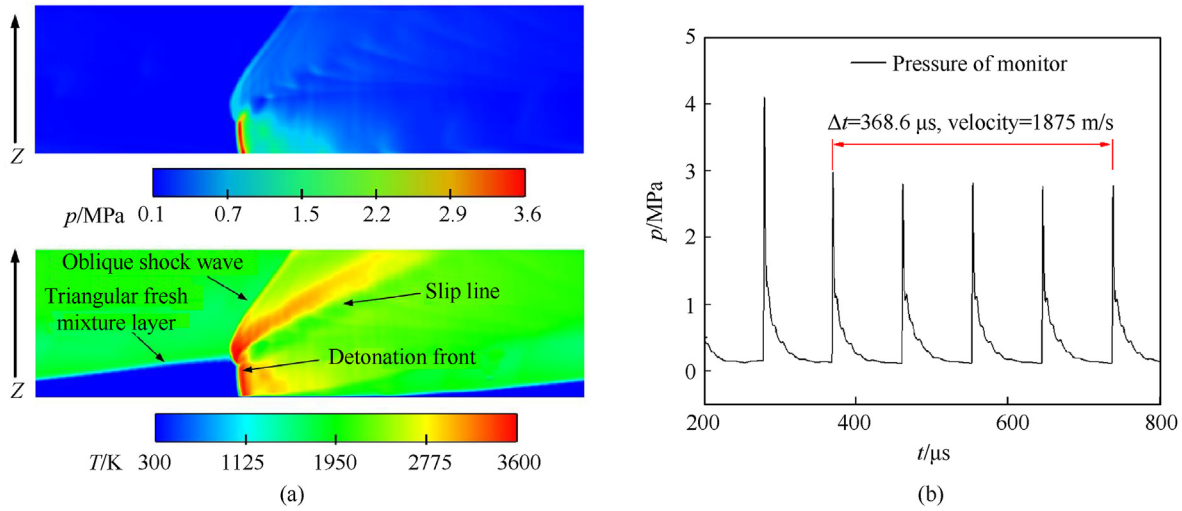

Fig. 5. Internal flow field of annular chamber: (a) Pressure and temperature contours; (b) Pressure curve at monitoring points.

$$F_{\text{wall}} = \iint_{\text{wall}} (p_{\text{wall}} - p_{\text{b}})\mathrm{d}A \tag{7}$$

$$F_{\text{total}} = F_{\text{chamber}} + F_{\text{wall}} \tag{8}$$

$$I_{\text{sp}} = \frac{F_{\text{total}}}{\dot{m} \cdot g} \tag{9}$$

In Eq. (6), F_{chamber} is the thrust generated by the outlet of chamber, ρ_{exit}, v_{axial} and p_{exit} are the gas density, gas axial velocity and static pressure at the outlet of the chamber respectively, and p_{b} is the ambient pressure; In Eq. (7), F_{wall} is the thrust generated by the end face of the inner wall and outer wall, where p_{wall} is the pressure on the end face of the inner wall and outer wall. In Eq. (9), I_{sp} is the specific impulse of fuel, F_{total} is the total thrust, $\dot{m}$ is the fuel mass flow rate, g is the gravity acceleration, which is 9.81 m/s^2. Fig. 6 is the thrust profile of each part of the annular chamber. It can be found that the thrust generated by the outlet of the combustion chamber is relatively stable, with an average value of 260.2 N. The thrust generated on the end face of the wall is negative and varies greatly, especially on the inner wall, which is caused by the negative pressure on the end face of inner and outer walls due to the suction effect [20]. The average total thrust generated by the annular chamber is 214.2 N and the fuel specific impulse is 3899.1 s.

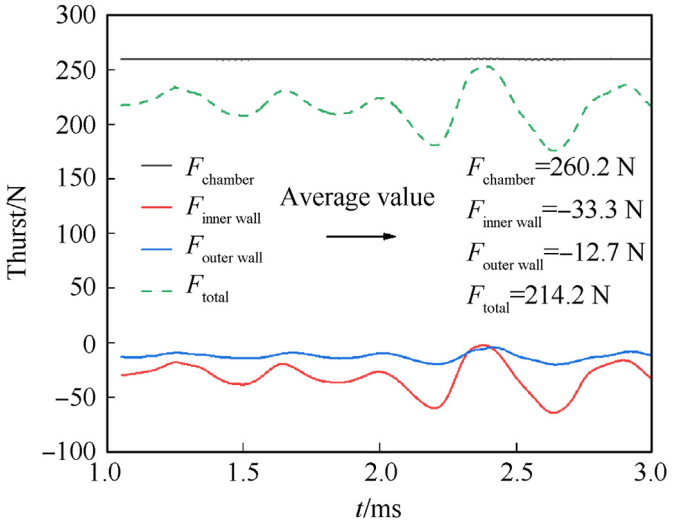

Fig. 6. Thrust performance of annular chamber.

As mentioned above, the detonation wave propagating in the circumferential direction at the head of the combustion chamber will produce non-axial air velocity, resulting in the existence of air velocity angle at the outlet of the chamber, which will causes a certain loss of kinetic energy. Fig. 7 shows the velocity vector distribution at the outlet of the annular chamber. The direction measured by the right-hand criterion is positive along the outlet direction of the annular chamber, and vice versa. It can be found that there are four typical velocity vector distribution regions at the outlet, which is marked as (a)-(b), and we named these four regions Collision Region, Isotropic Region, Axial Region and Reverse Region respectively. Fig. 7(b) is an enlarged view of the Collision Region, which is located at the downstream of oblique shock wave. This region is the junction between the oblique shock wave and the previous detonation cycle product. It can be found that the tangential velocity of the air flow at the oblique shock wave is in the same direction as the detonation wave rotation direction, while the tangential velocity of the air flow in the previous detonation cycle product is opposite to the detonation wave rotation direction, and velocity vector in the two directions collide in region 1. Fig. 7(a) is an enlarged view of the Isotropic Region, which follows by the oblique shock wave. And the tangential velocity of the air flow in this region is affected by the oblique shock wave, which is the same as the propagation direction of the rotating detonation wave. Fig. 7(c) shows the Axial Region, between region 2 and region 4, which is the intermediate transition section of the two regions, and the axial air velocity in this region is dominant. Fig. 7(d) shows the Reverse Region, before the oblique shock wave, and the tangential velocity of the air flow in this region is opposite to the propagation direction of the detonation wave. Interestingly, as shown in Fig. 8, we take the Aera-Weighted average value of tangential velocity at the outlet of the annular chamber and find that the average value is 87.5 m/s, which indicates that Reverse Region is dominant and tangential velocity at the outlet of the annular chamber is generally opposite to the propagation direction of the detonation wave. We will go for a more in-depth analysis below.

The momentum moment equation is applied to the exhausted gas in the chamber and integrated on the outlet plane to obtain the following expression:

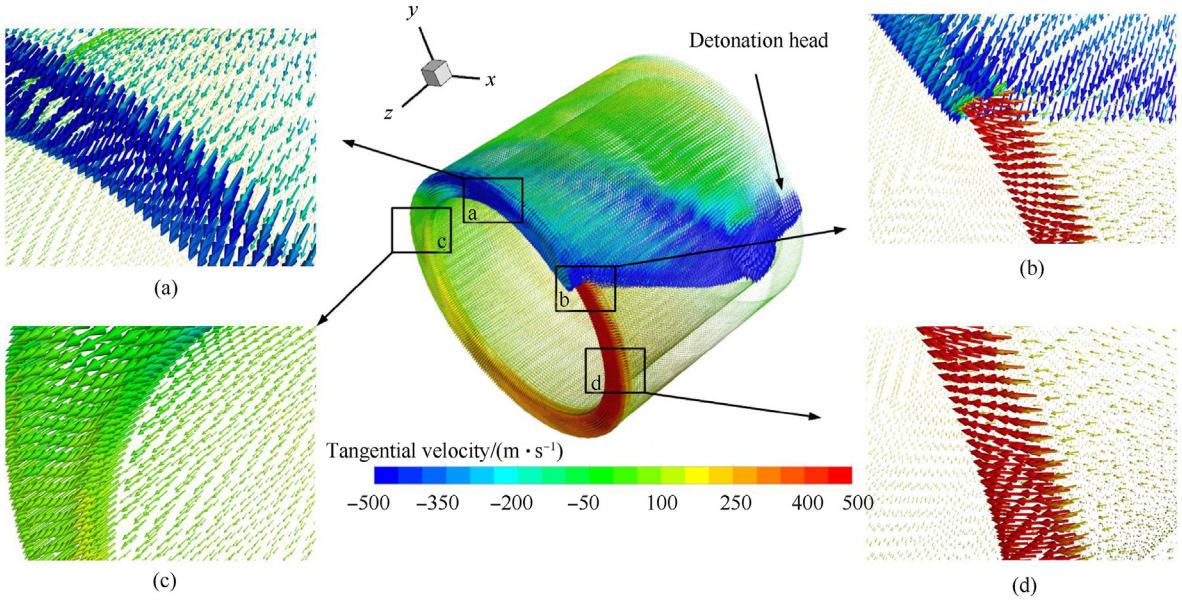

Fig. 7. Velocity vector distribution at the outlet of annular chamber: (a) Isotropic; (b) Collision Region; (c) Axial region; (d) Reverse region.

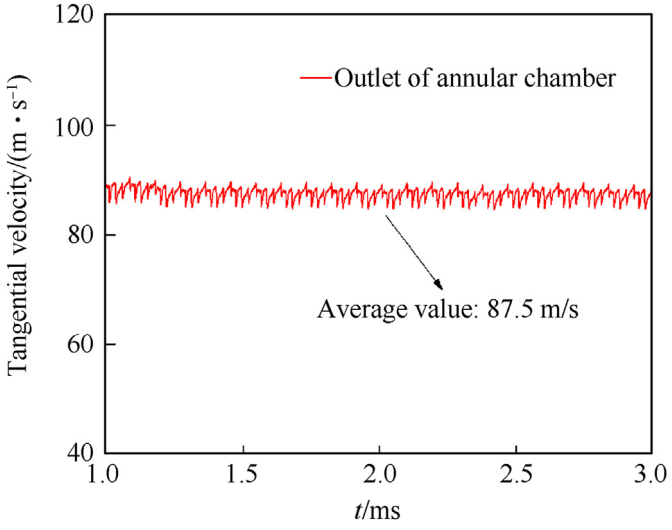

Fig. 8. Aera-Weighted average value of tangential velocity at the outlet of annular chamber.

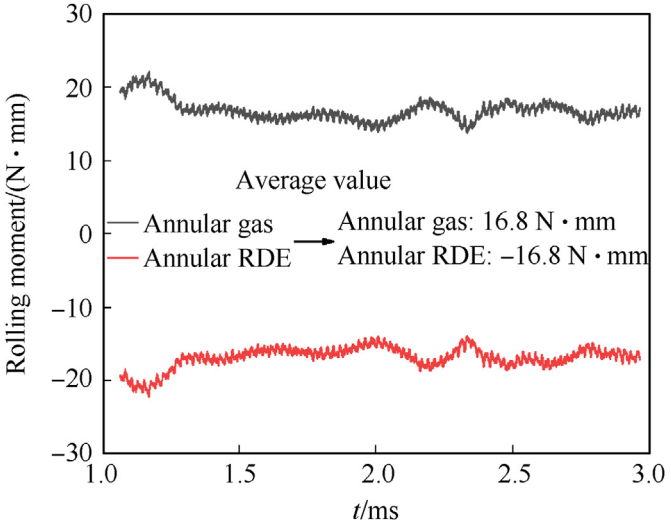

Fig. 9. Moment of annular.

$$M_{\text{gas}} = \iint_{\text{exit}} r\rho_{\text{exit}} v_{\text{tangential}} v_{\text{axial}} \mathrm{d}A \tag{10}$$

In the above equation, M_{gas} is the moment of exhausted gas, r is the force arm, which is the distance from the integration point to the central axis, $v_{\text{tangential}}$ is tangential component of total velocity at the outlet, the direction also follows the right-hand criterion, which the direction of chamber outlet is positive, and v_{axial} is the axial velocity at the outlet. Then the rolling moment acting on the annular chamber is equal to the M_{gas}, and the direction is opposite, which is

$$M_{\text{chamber}} = -M_{\text{gas}} \tag{11}$$

Fig. 9 is the time history curve of M_{chamber} and M_{gas}. It can be found that the direction of rolling moment received by the RDE is consistent with the rotation direction of the detonation wave, with an average value of −16.8 N mm, indicating that the rotating detonation wave will drive RDE to rotate in the same direction. While the moment received by the gas is opposite to RDE, which causes the tangential velocity at the outlet of the annular chamber to opposite to the propagation of the detonation wave. Because this paper adopted a simplified model, it can only give a qualitative rotation effect, and the specific rotation effect needs further clarifications.

The non-axial flow velocity at the outlet of the annular chamber not only results in the rolling moment of RDE, but also leads to the axial kinetic energy loss of RDE. The proportion of kinetic energy is calculated as following:

$$E_{\text{axial}} = \iint_{\text{exit}} \rho v_{\text{axial}}{}^2 \mathrm{d}A \Big/ \iint_{\text{exit}} \rho\left(v_{\text{axial}}{}^2 + v_{\text{tangential}}{}^2 + v_{\text{radial}}{}^2\right)\mathrm{d}A \tag{12}$$

$$E_{\text{tangential}} = \iint_{\text{exit}} \rho v_{\text{tangential}}{}^2 \mathrm{d}A \Big/ \iint_{\text{exit}} \rho\left(v_{\text{axial}}{}^2 + v_{\text{tangential}}{}^2 + v_{\text{radial}}{}^2\right)\mathrm{d}A \tag{13}$$

$$E_{\text{radial}} = \iint_{\text{exit}} \rho v_{\text{radial}}{}^2 \mathrm{d}A \Big/ \iint_{\text{exit}} \rho\left(v_{\text{axial}}{}^2 + v_{\text{tangential}}{}^2 + v_{\text{radial}}{}^2\right)\mathrm{d}A \tag{14}$$

where E_{axial}, $E_{\text{tangential}}$ and E_{radial} are the proportion of axial, tangential and radial kinetic energy respectively. $V_{\text{tangential}}$ and v_{radial} are the tangential and radial velocities of outlet respectively. In the annular chamber, the kinetic energy in these three directions accounts for 90.1%, 9.8% and 0.1% respectively, indicating that the main axial kinetic energy loss is caused by the tangential movement of the outlet air flow. The tangential velocity of the air flow converts the energy originally used to accelerate RDE into rotational kinetic energy of RDE, which will lead to unsatisfactory propulsion performance.

3.2. Hollow chamber

Similarly, we unwrapped the three-dimensional hollow chamber along the outer wall, and obtained the state of the flow field in the hollow chamber as showed in Fig. 10. On the contours of pressure and temperature, we can find there are three detonation waves in the flow field after stabilization, in which the peak of temperature and pressure are approximately 3800 K and 3 MPa respectively. By observing the temperature distribution, we find that the flow field is a typical triple wave structure, and there are still detonation waves, oblique shock waves, slip lines and triangular fresh mixture layer. Compared with the single wave flow field of Case 1, the detonation flow field in the hollow chamber is more complex, which is mainly caused by the configuration of hollow chamber. Because there is no restriction of the inner cylinder at the hollow chamber, a large amount of high-temperature and high-pressure gas is accumulated here, which makes the detonation wave more complex in the process of modal development and prone to multi-wave mode [19,33]. When there are multiple wave heads in the chamber, the consumption speed and filling speed of the fresh fuel layer will have a self-adjusting phenomenon [69], and the intensity of the detonation wave will change with the height of the fresh fuel layer, so the detonation flow field is more complex. Similarly, we set monitoring point (0, 19, 2) near the wall of hollow chamber to monitor the pressure curve, as showed in Fig. 10(b). We can discover that after ignition, the detonation wave in the flow field evolves from a single wave to triple waves. In addition, with more detonation waves, the pressure peak is significantly more irregular than Case 1, which will cause a large fluctuation in the gas flow velocity at the hollow chamber outlet. And v_{axial} is the square term in Eq. (5), which will cause the thrust of the hollow chamber to fluctuate more than that of the annular chamber, as we will show below.

Fig. 11 is the thrust profile of hollow chamber. Due to the flow field in the hollow chamber is more complex, it can also be seen that the thrust F_{chamber} fluctuates greatly, showing a form of significant oscillations. And there is no end face of the inner cylinder, F_{wall} is generated by the end face of the outer wall alone. Therefore,

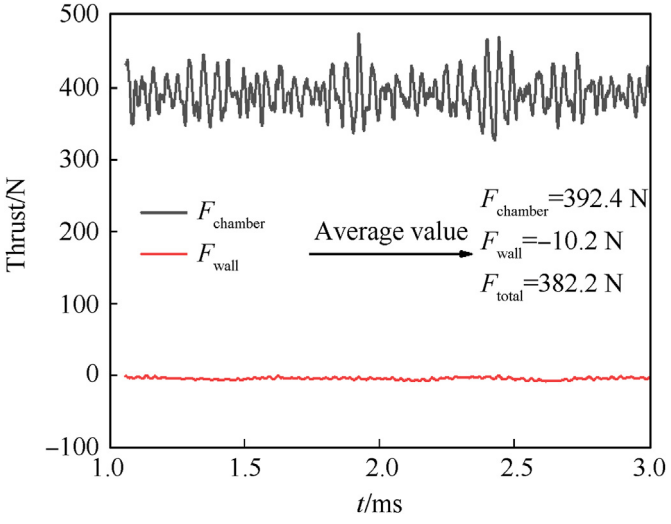

Fig. 11. Thrust performance of hollow chamber.

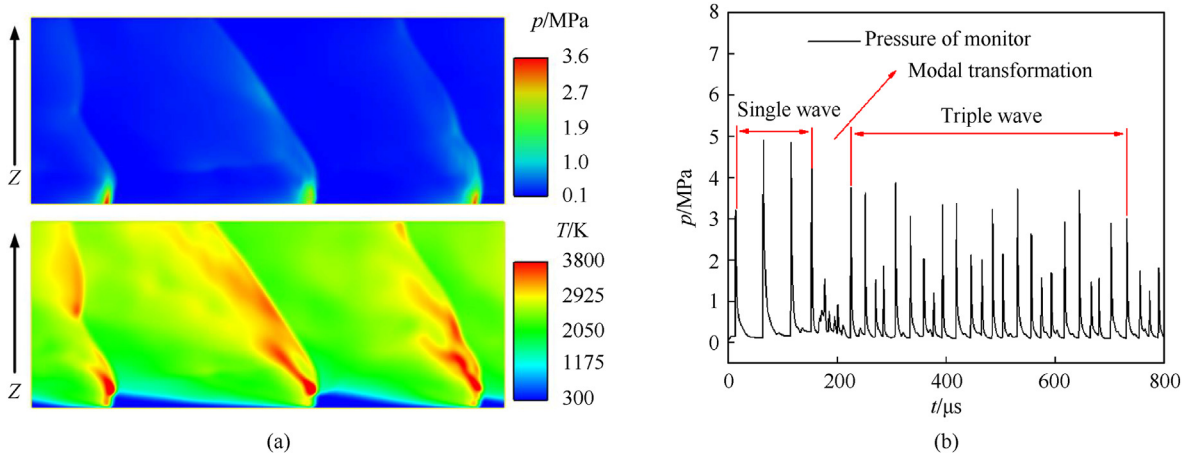

Fig. 10. Internal flow field of hollow chamber: (a) Pressure and temperature contours; (b) Pressure curve at monitoring points.

compared with the annular chamber, the negative thrust generated by this term is much lower, with an average value of −10.2 N, and is more stable. The total thrust of the hollow chamber is 382.2 N and the fuel specific impulse reaches 4642.8 s, which means that the smaller end face of the hollow chamber is one of the influence factor that reduce the thrust loss and improve the fuel specific impulse.

Because there are three rotating detonation waves in the hollow chamber, the velocity vector distribution at the outlet is more complicated than that in Case 1. Fig. 12 shows the velocity vector distribution of the hollow chamber. In this case, the detonation wave propagates in the positive direction. Firstly, according to the influence of three oblique shock waves, the outlet area of the chamber is divided into three areas by dotted lines as showed in the figure. It can be found that in the dotted line area affected by each oblique shock, there are still Collision Region, Isotropic Region, Axial Region and Reverse Region that have been observed in the previous section. Since the direction of detonation wave rotation is opposite to that of Case 1, the arrangement order of the four regions also changes, indicating that the four airflow velocity vector regions are caused by rotating detonation wave. From the enlarged view of air flow velocity vector, it can be found that the velocity vector distribution is more irregular compared to Case 1. This phenomenon may be caused by the change of the chamber or the increase of wave number, which needs further research. Similarly, according to Eq. (9) - Eq. (13), the rolling moment of the hollow chamber is 15.43 N mm, and the axial velocity kinetic energy, tangential velocity kinetic energy and radial velocity kinetic energy of the hollow chamber are 95.8%, 3.5% and 0.7% respectively. The axial kinetic energy of Case 2 is higher than Case 1, which is also one of the reasons for the higher fuel specific impulse.

3.3. Combined chamber

Fig. 13 shows the time-averaged Mach number contours of the external flow field of Case 1- Case 3, and the temperature and pressure curves are extracted on the central axis of the external flow field. In Fig. 13(a), We can find that after leaving the annular chamber, the air flow expands to about Mach 2, and begins to deflect inward, converges near the central axis of the external flow field, and the Mach number decreases gradually. It can be seen from the pressure and temperature distribution curve of the central axis that the pressure at the end face of the inner wall in the annular chamber is only 0.08 MPa, which is less than the ambient pressure of 0.1 MPa, and the temperature is reaching about 2350 K, indicating that low-pressure and high-temperature air mass is accumulated here. This is the reason for the F_{wall} mentioned above is negative, which is an important factor in the thrust loss of the annular chamber, and the combined chamber can better solve this problem. In Fig. 13(b) and Fig. 13(c), we can see that the Mach number in the area near the hollow chamber increases first, then decreases, and repeats this process. The difference is that in Fig. 13(c), the air flow generated by the annular chamber does not deflect inward, and the Mach number increases first and then decreases, but the repetition process can not be observed after a cycle, which appears to be integrated into the mainstream area. We select the external flow field structure in Fig. 13(c) for detailed analysis. The structure of free jet boundary and Mach disk can be clearly distinguished by observing the whole external flow field. It can be found from curve distribution that the pressure at the outlet of the combustion chamber is 0.16 MPa, which is higher than the ambient pressure, indicating that the flow field at the outlet of the combustion chamber is in the under-expansion state. Therefore, two expansion waves are generated at point A and point B, and continue to penetrate to the free boundary after interaction at point C. And the expansion wave is transformed into compression wave, and continues to extend to the free jet boundary after interaction at point F, so as to recycle and produce Mach disk structure.

Since the external flow field is not constrained by a profile, in order to describe its oscillation characteristics quantitatively, we set a monitoring point (50, 0,100) in the flow field of each case to record the pressure, and further introduce the relative standard deviation(*RSD*) [68], which can be calculated as follow:

$$RSD = \frac{\sqrt{\sum_i^N (p_i - \overline{p})^2 \Big/ (N-1)}}{\overline{p}} \tag{15}$$

where p_i is ith pressure, $\overline{p}$ is the time-average pressure, N is the total number of value point. As shown in Fig. 14, the pressure oscillation

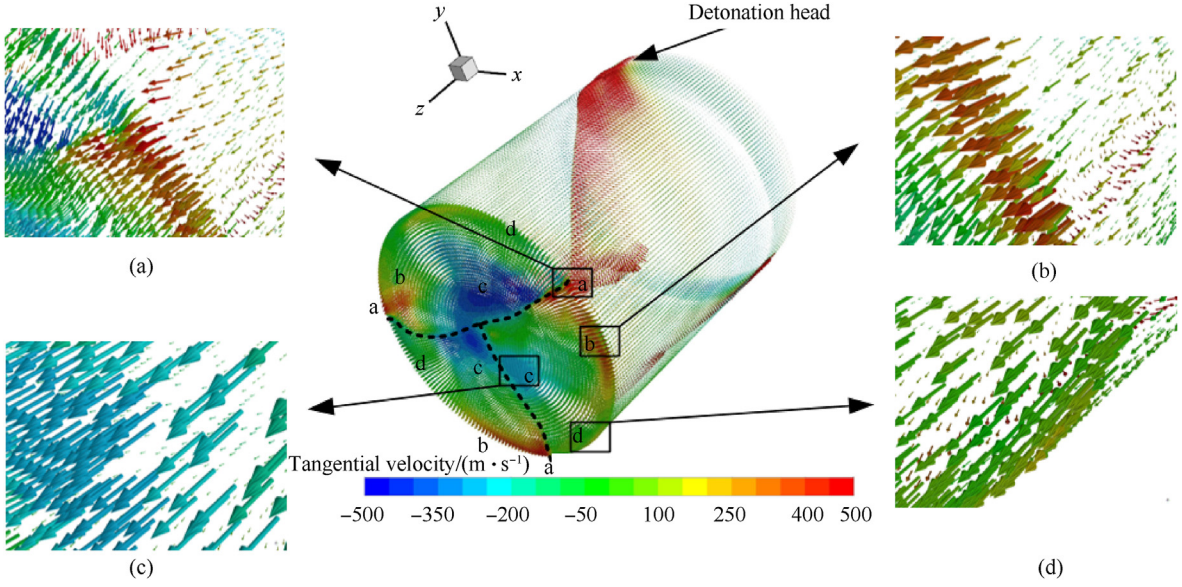

Fig. 12. Velocity vector distribution at the outlet of hollow chamber: (a) Collision region; (b) Isotropic region; (c) Reserve region; (d) Axial region.

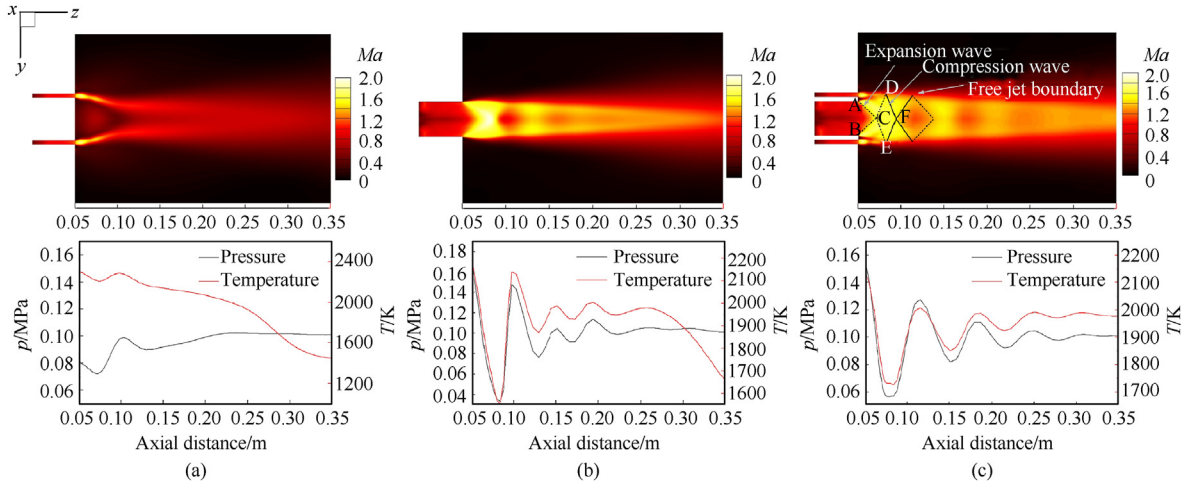

Fig. 13. External Flow field of (a) Case1, (b) Case 2; (c) Case 3.

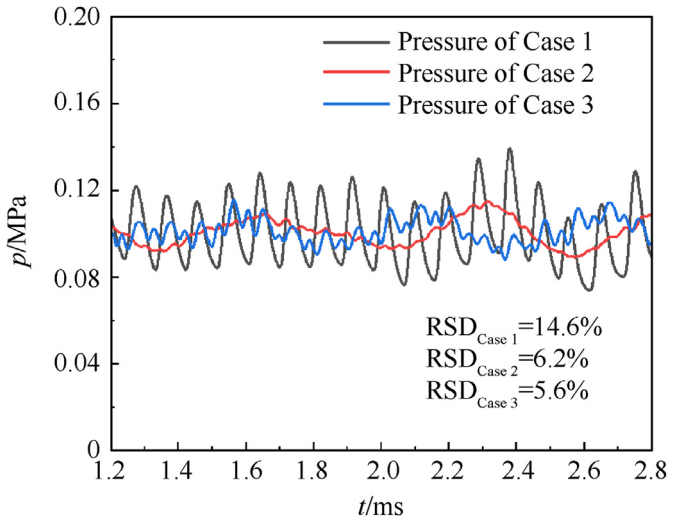

Fig. 14. Comparison of pressure oscillation characteristics of external flow field.

of Case 1 is strongest, changing from the range of 0.07–0.15 MPa, with a *RSD* of 14.6%. The oscillation frequency is 10790 Hz, which is almost the same as its detonation wave frequency(10822 Hz). It indicates that the oscillation signal is produced by the gradual degradation of the detonation wave in the combustion chamber, which is the reason of the detonation flow field has the characteristics of pressure oscillation. Because of the pressure oscillation of the detonation flow field, it is difficult to select a suitable design point in nozzle design. And at present, the time-averaged parameters are generally used as the design point [29,66]. However, this method has obvious disadvantages. The time-averaged design point is between the peak and trough of the oscillation parameter, therefore only a very short state makes the nozzle work at the design point, which leads to over-expansion or under-expansion of the nozzle in most of the time, which greatly reduces the efficiency of the nozzle. By observing the pressure signal of Case 3, we can find that the oscillation range of pressure is significantly reduced compared to Case 1, fluctuating between 0.09 MPa and 0.12 MPa, and its *RSD* is the minimum value of 5.6% among the three cases, indicating that the flow field after combination is more uniform. The combined chamber permits using fluid to adjust the pressure oscillation of detonation flow field, and is conducive to the selection of nozzle design points. This result shows that the effect of reducing the oscillation characteristics of detonation flow field through the interaction of detonation flow field without mechanical nozzle is feasible, which is of profound significance to the nozzle design of RDE.

Table 2 shows the comparison of propulsion performance for all the three cases. In terms of thrust performance, the thrust increases from Case 1 to Case 3 since the thrust is related to the mass flow rate of premixed gas. However, the thrust value of Case3 is higher than the sum of Case 1 and Case 2. This is because the hollow chamber replaces the end face of the annular chamber in Case 3, which makes the original negative thrust of this part disappear, thus improves the thrust performance and makes the RDE structure more compact. In terms of the specific impulse performance, it can be found that Case 2 has the highest specific impulse, Case 3 is slightly lower, and Case 1 is the smallest. And in terms of rolling moment and axial kinetic energy ratio, we can find that although the rolling moment of Case 3 is reduced to −1.4 N mm, which is almost negligible, its axial kinetic energy ratio is still lower than that of Case 2. This is because the nozzle is not designed at the outlet of the combined chamber in this paper, and the air flow directly enters the external field for interaction. And the calculation parameters of axial kinetic energy ratio are selected at the outlet of chamber, so that it can not reflect the performance improvement. The smaller rolling moment is because the moment of the hollow and annular chambers cancel out each other, indicating the outlet air flow of Case 3 is reversed. If the nozzle is added to make the outlet air flow mix with each other and discharge, it can effectively reduce the non-axial air flow velocity, and increase the proportion of axial kinetic energy, improve the propulsion performance and simulate the potential of RDE.

4. Conclusions

Detailed internal and external flow field structures of annular chamber, hollow chamber and combined chamber are obtained by three-dimensional numerical simulations in this paper. The equation of rolling moment is formulated, and the propulsion performance of each case is obtained.

Finally, through the new configuration of combined chamber, it is proved that the method of adjusting the pressure oscillation characteristics of detonation flow field through the interaction of detonation flow field is feasible.

For the internal flowfield, four velocity vector regions are

Table 2
Comparison of propulsive performance of each case.

Case	Mass flow rate/(kg·s^{-1})	Thrust/N	Fuel specific impulse/s	Rolling moment/(N·mm)	E_{axial}/%
1	0.2	214.2	3899.1	−16.8	90.1
2	0.3	382.2	4642.8	15.4	95.8
3	0.5	625.6	4559.8	−1.4	93.1

summarized at the outlet of the chamber, which are named as Collision Region, Isotropic Region, Axial Region and Reverse Region. Averaging the tangential velocity at the outlet, it is found that the airflow velocity vector at the outlet is opposite to the direction of detonation wave propagation. It is found that the non-axial velocity leads to the loss of axial kinetic energy of RDE, which makes RDE subject to the rolling moment in the tangential direction. In the annular chamber, the non-axial kinetic energy accounts for 9.9% and the rolling moment is 16.8 N mm.

In the external flow field of Case2 and Case3 in this paper, it is found that the expansion wave and compression wave are reflected on the free jet boundary and producing the Mach disk structure. The pressure oscillation characteristics of each case are analyzed. It is found that the external flow field of the combined chamber is more stable compared with the annular chamber and hollow chamber. It shows that the idea of fluid regulation is feasible to weaken the inherent pressure oscillation characteristics of the detonation flow field, which is of great significance for the flow field regulation and nozzle design of RDE.

Because the nozzle design of combined chamber is not carried out in this paper, and only the combined chamber of 0.5 kg/s was simulated, the performance of the combined chamber may not reach the best state. Later, if the combined chamber with different mass flow rate is studied with the nozzle, it can be predictable that the combined chamber can not only make the nozzle reach a better design state because of its small pressure oscillation, but also has the potential to reduce the proportion of non-axial kinetic energy, which can further improve the propulsion performance and simulate the potential of RDE.

Declaration of competing interest

The authors declare that they have no known competing financial interests or personal relationships that could have appeared to influence the work reported in this paper.

References

[1] Kailasanath K. Review of propulsion applications of detonation waves. AIAA J 2000;38(9):1698–708. https://doi.org/10.2514/2.1156.
[2] Ma JZ, Luan MY, Xia ZJ, Wang JP, Wang B. Recent progress, development trends, and consideration of continuous detonation engines. AIAA J 2020;58(12):4976–5035. https://doi.org/10.2514/1.J058157.
[3] Kailasanath K. The rotating detonation-wave engine concept: a brief status report. In: 49th AIAA aerospace sciences meeting including the new horizons forum and aerospace exposition; 2011. Orlando, FL.
[4] Braun EM, Lu FK, Wilson DR, Camberos JA. Airbreathing rotating detonation wave engine cycle analysis. Aero Sci Technol 2013;27(1):201–8. https://doi.org/10.2514/6.2010-7039.
[5] Voitsekhovskii BV, V Mitrofanov V, Topchiyan ME. Structure of the detonation front in gases (survey). Combust Explos Shock Waves 1969;5(3):267–73.
[6] Nlcholls JA, Cullen RE, Ragland KW. Feasibility studies of a rotating detonation wave rocket motor. J Spacecraft Rockets 1966;3(6):893–8.
[7] Kindracki J, Wolanski P, Gut Z. Experimental research on the rotating detonation in gaseous fuels–oxygen mixtures. Shock Waves 2011;21(2):75–84. https://doi.org/10.1007/s00193-011-0298-y.
[8] Rankin BA, Hoke J, Schauer F. Periodic exhaust flow through a converging-diverging nozzle downstream of a rotating detonation engine. In: 52nd aerospace sciences meeting. Maryland: National Harbor; 2014. https://doi.org/10.2514/6.2014-1015.
[9] Lu FK, Braun EM. Rotating detonation wave propulsion: experimental challenges, modeling, and engine concepts. J Propul Power 2014;30(5):1125–42. https://doi.org/10.2514/1.B34802.
[10] Davidenko DM, Gokalp I, Kudryavtsev AN. Numerical simulation of the continuous rotating hydrogen-oxygen detonation with a detailed chemical mechanism. In: Proceedings of the West-East high speed flow field conference; 2007. Moscow, Russia.
[11] Davidenko DM, Gokalp I, Kudryavtsev AN. Numerical study of the continuous detonation wave rocket engine. In: 15th AIAA international space planes and hypersonic systems and technologies conference. Ohio: Dayton; 2008. https://doi.org/10.2514/6.2008-2680.
[12] Kindracki J, Kobiera A, Wolański P, Gut Z, Swiderski K. Experimental and numerical study of the rotating detonation engine in hydrogen-air mixtures. Progr Propul Phys 2011;2:555–82. https://doi.org/10.1051/eucass/201102555.
[13] Wang F, Weng CS, Wu YW, Bai QD, Xu H. Effects of total pressures and equivalence ratios on kerosene/air rotating detonation engines using a paralleling CE/SE method. Def Technol 2021;17(6):1805–16. https://doi.org/10.1016/j.dt.2020.09.015.
[14] Zheng Q, Meng HL, Weng CS, Wu YW, Feng WK, Wu ML. Experimental research on the instability propagation characteristics of liquid kerosene rotating detonation wave. Def Technol 2020;16(6):1106–15. https://doi.org/10.1016/j.dt.2020.06.028.
[15] Zheng Q, Weng CS, Bai QD. Experimental research on the propagation process of continuous rotating detonation wave. Def. Technol 2013;9(4):201–7. https://doi.org/10.1016/j.dt.2013.11.003.
[16] Rankin BA, Fotia M, Paxson DE, Hoke J, Schauer F. Experimental and numerical evaluation of pressure gain combustion in a rotating detonation engine. In: 53rd AIAA aerospace sciences meeting. Florida: Kissimmee; 2015. https://doi.org/10.2514/6.2015-0877.
[17] Anand V, George AC St, Driscoll RB, Gutmark EJ. Statistical treatment of wave instability in rotating detonation combustors. In: 53rd AIAA aerospace sciences meeting. Florida: Kissimmee; 2015.
[18] Ishihara K, Matsuoka K, Kasahara J, Matsuo A, Funaki I. Performance evaluation of a rotating detonation engine with conical-shape tail. In: 53rd AIAA aerospace sciences meeting. Florida: Kissimmee; 2015. https://doi.org/10.2514/6.2015-0630.
[19] Sun J, Zhou J, Liu SJ, Lin ZY, Lin W. Numerical investigation of a non-premixed hollow rotating detonation engine. Int J Hydrogen Energy 2019;44(31):17084–94. https://doi.org/10.1016/j.ijhydene.2019.04.168.
[20] Sun J, Zhou J, Liu SJ, Lin ZY, Lin W. Plume flowfield and propulsive performance analysis of a rotating detonation engine. Aero Sci Technol 2018;81:383–93. https://doi.org/10.1016/j.ast.2018.08.024.
[21] Schwer DA, Brophy CM, Kelso RH. Pressure characteristics of an aerospike nozzle in a rotating detonation engine. In: 2018 joint propulsion conference; 2018. https://doi.org/10.2514/6.2018-4968. Cincinnati, Ohio.
[22] Sun CW, Zheng HT, Zhao NB, Li ZM, Zhu WL. Performance evaluation and outlet load improvement of a rotating detonation combustor with different outlet nozzles. Int J Hydrogen Energy 2021;46(35):18644–60. https://doi.org/10.1016/j.ijhydene.2021.02.213.
[23] Fotia ML, Schauer F, Kaemming T, Hoke J. Experimental study of the performance of a rotating detonation engine with nozzle. J Propul Power 2016;32(3):674–81. https://doi.org/10.2514/1.B35913.
[24] Braun J, Saracoglu BH, Paniagua G. Unsteady performance of rotating detonation engines with different exhaust nozzles. J Propul Power 2017;33(1):121–30. https://doi.org/10.2514/1.B36164.
[25] Bach E, Bohon MD, Paschereit CO, Stathopoulos P. Impact of outlet restriction on RDC performance and stagnation pressure rise. In: AIAA scitech 2019 forum. San Diego: California; 2019. https://doi.org/10.2514/6.2019-0476.
[26] Frolov SM, Aksenov VS, Gusev PA, Ivanov VS, Shamshin IO. Zel'dovich thermodynamic cycle and perspectives of its application in chemical ramjet and rocket propulsion. In: Accomplishments in the combustion science in the last decade; 2014. p. 156–61.
[27] Schnabel MC, Brophy CM. Pressure distribution and performance impacts of aerospike nozzles on rotating detonation engines. In: 2018 AIAA aerospace science metting; 2018. https://doi.org/10.2514/6.2018-1626. Kissimmee, Florida.
[28] Wei WL, Wu YW, Weng CS, Zheng Q. Influence of propagation direction on operation performance of rotating detonation combustor with turbine guide vane. Def Technol 2021;17(5):1617–24. https://doi.org/10.1016/j.dt.2020.08.009.
[29] Huang Y, Xia HQ, Chen XN, Luan ZY, You YC. Shock dynamics and expansion characteristics of an aerospike nozzle and its interaction with the rotating detonation combustor. Aero Sci Technol 2021;117:106969. https://doi.org/10.1016/j.ast.2021.106969.
[30] Zhang QB, Wang K, Dong RX, Fan W, Lu W, Wang YJ. Experimental research on

propulsive performance of the pulse detonation rocket engine with a fluidic nozzle. Energy 2019;166:1267–75. https://doi.org/10.1016/j.energy.2018.10.165.
[31] Zhang QB, Wang K, Wang JG, Qiao XQ, Fan W. Experimental research on vector control features of a pulse detonation tube with fluidic nozzle. Aero Sci Technol 2021:106456. https://doi.org/10.1016/j.ast.2020.106456.
[32] Tang XM, Wang JP, Shao YT. Three-dimensional numerical investigations of the rotating detonation engine with a hollow combustor. Combust Flame 2015;162(4):997–1008. https://doi.org/10.1016/j.combustflame.2014.09.023.
[33] Xia ZJ, Tang XM, Luan MY, Zhang SJ, Ma Z, Wang JP. Numerical investigation of two-wave collision and wave structure evolution of rotating detonation engine with hollow combustor. Int J Hydrogen Energy 2018;43(46):21582–91. https://doi.org/10.1016/j.ijhydene.2018.09.165.
[34] Liu XY, Chen YL, Xia ZJ, Wang JP. Numerical study of the reverse-rotating waves in rotating detonation engine with a hollow combustor. Acta Astronaut 2020;170:421–30. https://doi.org/10.1016/j.actaastro.2020.02.008.
[35] Anand V, George AS, de Luzan CF, Gutmark E. Rotating detonation wave mechanics through ethylene-air mixtures in hollow combustors, and implications to high frequency combustion instabilities. Exp Therm Fluid Sci 2018;92:314–25. https://doi.org/10.1016/j.expthermflusci.2017.12.004.
[36] Yokoo R, Goto K, Kasahara J, et al. Experimental study of internal flow structures in cylindrical rotating detonation engines. Proc Combust Inst 2021;38(3):3759–68. https://doi.org/10.1016/j.proci.2020.08.001.
[37] Wang YH, Le JL. A hollow combustor that intensifies rotating detonation. Aero Sci Technol 2019;85:113–24. https://doi.org/10.1016/j.ast.2018.12.014.
[38] Liu SJ, Huang SY, Peng HY, Yuan XQ. Characteristics of methane-air continuous rotating detonation wave in hollow chambers with different diameters. Acta Astronaut 2021;183:1–10. https://doi.org/10.1016/j.actaastro.2021.02.035.
[39] Peng HY, Liu WD, Liu SJ, Zhang HL, Jiang LX. Hydrogen-air, ethylene-air, and methane-air continuous rotating detonation in the hollow chamber. Energy 2020;211:118598. https://doi.org/10.1016/j.energy.2020.118598.
[40] Wang YH, Le JL. A hollow combustor that intensifies rotating detonation. Aero Sci Technol 2019;85:113–24. https://doi.org/10.1016/j.ast.2018.12.014.
[41] Zhang HL, Jiang LX, Liu WD, Liu SJ. Characteristic of rotating detonation wave in the H_2/Air hollow chamber with Laval nozzle. Int J Hydrogen Energy 2021;46(24):13389–401. https://doi.org/10.1016/j.ijhydene.2021.01.143.
[42] Sun J, Zhou J, Liu SJ, Lin ZY, Lin W. Numerical investigation of a non-premixed hollow rotating detonation engine. Int J Hydrogen Energy 2019;44(31):17084–94. https://doi.org/10.1016/j.ijhydene.2019.04.168.
[43] Sun J, Zhou J, Liu SJ, Lin ZY, Cai JH. Effects of injection nozzle exit width on rotating detonation engine[J]. Acta Astronaut 2017;140:388–401. https://doi.org/10.1016/j.actaastro.2017.09.008.
[44] Yang CL, Ma H, Wu XS, Xu XY. A computational and experimental study of injection structure effect on H_2-air rotating detonation engine. In: 52nd AIAA/SAE/ASEE joint propulsion conference; 2016. https://doi.org/10.2514/6.2016-4571. Salt Lake City, UT.
[45] B Yao S, Ma Z, Zhang SJ, Luan MY, Wang JP. Reinitiation phenomenon in hydrogen-air rotating detonation engine. Int J Hydrogen Energy 2017;42(47):28588–98. https://doi.org/10.1016/j.ijhydene.2017.09.015.
[46] B Yao S, Tang XM, Wang JP, Shao YT, Zhou R. Three-dimensional numerical study of flow particle paths in rotating detonation engine with a hollow combustor. Combust Sci Technol 2017;189(6):965–79. https://doi.org/10.1080/00102202.2016.1264941.
[47] Schwer DA, Kailasanath K. Modeling exhaust effects in rotating detonation engines. In: 48th AIAA/ASME/SAE/ASEE joint propulsion conference & exhibit; 2012. https://doi.org/10.2514/6.2012-3943. Atlanta, Georgia.
[48] B Yao S, Wang JP. Multiple ignitions and the stability of rotating detonation waves. Appl Thermal Eng 2016;108:927–36. https://doi.org/10.1016/j.applthermaleng.2016.07.166.
[49] Shao YT, Liu M, Wang JP. Continuous detonation engine and effects of different types of nozzle on its propulsion performance. Chin J Aeronaut 2010;23:647–52. https://doi.org/10.1016/S1000-9361(09)60266-1.
[50] Jourdaine N, Tsuboi N, Ozawa K, Kojima T, Hayashi AK. Three-dimensional numerical thrust performance analysis of hydrogen fuel mixture rotating detonation engine with aerospike nozzle. Proc Combust Inst 2019;37(3):3443–51. https://doi.org/10.1016/j.proci.2018.09.024.
[51] Kurita N, Jourdaine NH, Tsuboi N, Ozawa K, Hayashi AK, Kojima T. In: Three-dimensional numerical simulation on hydrogen/air rotating detonation engine with aerospike nozzle: effects of nozzle geometries. Orlando, FL: AIAA SciTech 2020 Forum; 2020. https://doi.org/10.2514/6.2020-0688.
[52] Tsuboi N, Jourdaine NH, Watanabe T, Hayashi AK, Kojima T. Three-dimensional numerical simulation on hydrogen-oxygen rotating detonation engine with unchoked aerospike nozzle. In: 2018 AIAA aerospace sciences meeting; 2018. https://doi.org/10.2514/6.2018-1885. Kissimmee, Florida.
[53] Zheng YS, Wang C, Xiao BG, Liu Y, Cai JH. Numerical simulation of radial-stratified rotating detonation flow field structures with different injection patterns. Int J Hydrogen Energy 2020;45(56):32619–31. https://doi.org/10.1016/j.ijhydene.2020.09.005.
[54] Meng QY, Zhao NB, Zheng HL, Yang JL, Qi L. Numerical investigation of the effect of inlet mass flow rates on H_2/air non-premixed rotating detonation wave. Int J Hydrogen Energy 2018;43(29):13618–31. https://doi.org/10.1016/j.ijhydene.2018.05.115.
[55] Liu PX, Guo QL, Sun D, Li C, Zhang HX. Wall effect on the flow structures of three-dimensional rotating detonation wave. Int J Hydrogen Energy 2020;45(53):29546–59. https://doi.org/10.1016/j.ijhydene.2020.07.196.
[56] Wu KW, Zhang SJ, Luan MY, Wang JP. Effects of flow-field structures on the stability of rotating detonation ramjet engine. Acta Astronaut 2020;168:174–81. https://doi.org/10.1016/j.actaastro.2019.12.022.
[57] Zhao NB, Meng QY, Zheng HT, Li ZM, Deng FQ. Numerical study of the influence of annular width on the rotating detonation wave in a non-premixed combustor. Aero Sci Technol 2020;100:105825. https://doi.org/10.1016/j.ast.2020.105825.
[58] Shao YT, Liu M, Wang JP. Numerical investigation of rotating detonation engine propulsive performance. Combust Sci Technol 2010;182(11–12):1586–97. https://doi.org/10.1080/00102202.2010.497316.
[59] Zhou R, Wang JP. Numerical investigation of shock wave reflections near the head ends of rotating detonation engines. Shock Waves 2013;23(5):461–72. https://doi.org/10.1007/s00193-013-0440-0.
[60] Wu D, Zhou R, Liu M, Wang JP. Numerical investigation of the stability of rotating detonation engines. Combust Sci Technol 2014;186(10–11):1699–715. https://doi.org/10.1080/00102202.2014.935641.
[61] Ma FH, Choi JY, Yang V. Propulsive performance of airbreathing pulse detonation engines. J Propul Power 2006;22(6):1188–203. https://doi.org/10.2514/1.21755.
[62] Bykovskii FA, Zhdan SA, Vedernikov EF. Continuous spin detonations. J Propul Power 2006;22(6):1204–16. https://doi.org/10.2514/1.17656.
[63] Smirnov NN, Betelin VB, Nikitin VF, Stamov LI, Altoukhov DI. Accumulation of errors in numerical simulations of chemically reacting gas dynamics. Acta Astronaut 2015;117:338–55. https://doi.org/10.1016/j.actaastro.2015.08.013.
[64] Smirnov NN, Betelin VB, Shagaliev RM, Nikitin VF, Bekyakov IM, Deryuguin YN, Aksenov SV, Korchazhkin DA. Hydrogen fuel rocket engines simulation using LOGOS code. Int J Hydrogen Energy 2014;39(20):10748–56. https://doi.org/10.1016/j.ijhydene.2014.04.150.
[65] Wang F, Weng CS, Wu YW, Bai QD, Zheng Q, Xu H. Numerical research on kerosene/air rotating detonation engines under different injection total temperatures. Aero Sci Technol 2020;103:105899. https://doi.org/10.1016/j.ast.2020.105899.
[66] Zhu YY, Wang K, Wang ZC, Zhao MH, Jiao ZT, Wang Y, Fan W. Study on the performance of a rotating detonation chamber with different aerospike nozzles. Aero Sci Technol 2020;107:106338. https://doi.org/10.1016/j.ast.2020.106338.
[67] Menter FR. Two-equation eddy-viscosity turbulence models for engineering applications. AIAA J 1994;32(8):1598–605. https://doi.org/10.2514/3.12149.
[68] Meng HL, Xiao Q, Feng WK, Wu ML, Han XP, Wang F, Weng CS, Zheng Q. Air-breathing rotating detonation fueled by liquid kerosene in cavity-based annular combustor. Aero Sci Technol 2022;107407. https://doi.org/10.1016/j.ast.2022.107407.
[69] Liu YS, Wang YH, Li Ys, Li Y, Wang JP. Spectral analysis and self-adjusting mechanism for oscillation phenomenon in hydrogen-oxygen continuously rotating detonation engine, Chin. J. Aeronaut. 2015;28:1–9. https://doi.org/10.1016/j.cja.2015.03.006.